Characterization of the Morphological and Synaptic Properties of Terminals in Koniocellular versus Magnocellular/Parvocellular Parallel Pathways in the Lateral Geniculate Nucleus of the Tree Shrew (*Tupaia belangeri)*

Francesca Paris Sciaccotta
Charlottesville, Virginia

B.A., Miami University, 2019

Predissertation presented to the Graduate Faculty
of the University of Virginia in Candidacy for the Degree of
Master of Arts

Department of Psychology

University of Virginia
December, 2021

Abstract

In addition to its main excitatory input coming from the retina, the lateral geniculate nucleus (LGN) of the thalamus receives axons from the superior colliculus (SC). In tree shrews (*Tupaia belangeri*), these tectogeniculate (TG) projections terminate in the koniocellular laminae 3 and 6, but their precise role in this pathway is unknown. To address the circuitry that underlines the TG input regulation of geniculate relay, I studied the synaptic circuitry in koniocellular laminae and its differences from those in magnocellular and parvocellular laminae. In particular, I characterized the ultrastructural and connective properties of retinal and SC terminals across these laminae in the LGN of tree shrews. Electron microscopy analysis to categorize the morphological and synaptic characteristics of these LGN terminals revealed that the terminals in both koniocellular and magno/parvo laminae display a multi-modal distribution, indicating inputs from various origins. Immuno-EM experiments revealed that the largest size subpopulation of terminals contained VGLUT2 and formed large synaptic zones with thick postsynaptic density primarily onto dendrites in laminae 1 and 2, and primarily onto vesicle-filled, presumed interneuronal profiles in lamina 6. Triadic arrangements were seen in both sets of laminae, however, they were more prevalent in VGLUT2+ terminals in lamina 6. VGLUT2+ terminals in lamina 6 were smaller, had less visible protrusions, made less synaptic contacts, and consisted of two distinct subpopulations of terminal sizes. These findings provide evidence that the morphological and connective characteristics of synaptic circuitry in the tree shrew LGN laminae differ based on their parallel pathway segregation. Furthermore, the differences between these parallel pathways may be due, in part, by the TG inputs that project to koniocellular laminae.

Introduction

The superior colliculus (SC), or optic tectum (OT) in non-mammalian species, is a critical node in the network responsible for reorienting an organism towards objects of interest. While

the output of the SC is going to various places, including pulvinar (Albano, Norton, & Hall, 1979; Benevento & Standage, 1983), parabigeminal nucleus (Wang, Takatsuji, Yamano, & Tohyama, 1988; Feig & Harting, 1992), and brainstem nuclei (Grantyn & Grantyn, 1982) to carry out this function, there is an input to the lateral geniculate nucleus (LGN) of the thalamus that has been sparsely studied, which raises the question of how the role of the SC is mediated through this thalamic network. Given that more recent findings are highlighting the potential role of the SC in target selection (Basso & Wurtz, 1998; Li & Basso, 2005), attention (Li & Basso, 2008; Lovejoy & Krauzlis, 2010; Zenon & Krauzlis, 2012), and decision making (Horwitz, Batista, & Newsome, 2004; Lo & Wang, 2006), it is critical to investigate if and how these tectogeniculate (TG) projections may be organized relative to the circuitry that mediates visual sensory perception, and its contributions to the higher cognitive functions of decision making and attention. To start addressing this, I conducted experiments to characterize the morphological and synaptic circuitry properties of TG terminals in the context of the parallel pathways in geniculate laminae.

In mammals, the SC is a large, layered structure found at the dorsal surface (tectum) of the midbrain. These layers are functionally segregated into two divisions: a dorsally located visuosensory division and a ventrally located motor division (Sparks & Hartwich-Young, 1989; May, 2006). The cells in the superficial layers of the SC are specialized to receive retinal information, as well as potentially parabigeminal (PBG) and internal axons, and those cells then project to the dorsal lateral geniculate nucleus (dLGN) of the thalamus (Graybiel, 1975 [cat]; Pollack & Hickey, 1979 [monkey]; Graham & Casagrande, 1980 [tree shrew]; Lund, Land, & Boles, 1980 [rat]; Petry, Agarwala, & May III, 1989 [squirrel]; Zhang & Hoffmann, 1993 [ferret]; Figure 1). SC axon projection patterns to geniculate laminae have been identified in a variety of mammalian species, including primates, cats, ferrets, tree shrews, rabbits, and rodents (Stanford, Friedlander, & Sherman, 1981; Harting, Updyke, & Van Lieshout, 1991; Lachica & Casagrande, 1993; Bickford, Zhou, Krahe, Govindaiah, & Guido, 2015). In particular, TG axons innervated a distinct set of geniculate laminae in each species, suggesting that TG axons are

closely associated with layers that contain W-type relay cells (Stanford et al., 1981; Harting et al., 1991; Lachica & Casagrande, 1993; Bickford et al., 2015). More recent studies provided further evidence that the TG pathway is a component of a distinct visual channel across species: Bickford et al. (2015) demonstrated, using optogenetic, *in vitro* physiological, and electron microscopy techniques, that the mouse dorsolateral shell of the dLGN receives two distinct sources of direction-selective signals, one from the retina and the other from the SC. They revealed that both retinothalamic (RT) and TG terminals converge to innervate a distinct class of relay cells that are identified as W-like (Bickford et al., 2015). This provides further evidence that the TG pathway is a component of a distinct, W- or konio-like visual channel across species.

The parallel pathways in dLGN have been heavily characterized. In most species, the LGN of the thalamus is organized into laminae which are devoted to one or more parallel processing streams (Campbell, Jane, & Yashon, 1967 [tree shrew, hedgehog]; Kaas, Huerta, Weber, & Harting, 1978 [primate]; Holdefer & Norton, 1995 [tree shrew]; Hendry & Reid, 2000 [primate]; Van Horn, Erişir, & Sherman, 2000 [cat]; Kaplan, 2004, 2014 [primate]; Kerschensteiner & Guido, 2017 [mouse]). In primates, tree shrews, and some carnivores, parallel processing streams originating from the retina remain segregated in the LGN. The parallel pathways that are segregated in geniculate laminae include ipsilateral versus contralateral input, ON versus OFF-center receptive fields, and magnocellular versus parvocellular versus koniocellular pathways (Campbell et al., 1967; Holdefer & Norton, 1995; Kaplan, 2004, 2014). Although, segregation of these parallel pathways can differ across species. For example, in the six-layered primate LGN there are layers that are devoted to particular retinal ganglion cell (RGC) input: the two most ventral layers (1-2) are the magnocellular (M) layers, which contain large cells that primarily receive input from parasol

RGCs (Leventhal, Rodieck, & Dreher, 1981; Perry, Oehler, & Cowey, 1984); the four dorsal layers (3-6) are the parvocellular (P) layers, which contain smaller cells that receive input from midget ganglion cells (Leventhal et al., 1981; Perry et al., 1984; Rodieck & Watanabe, 1993); and the smallest relay cells, koniocellular (K) cells, are found in the interlaminar zones and form three pairs of K layers which receive direct retinal input from small-sized RGCs and indirect retinal input from the superior colliculus (Kaas et al., 1978; Lachica & Casagrande, 1993; Casagrande, 1994; Hendry & Reid, 2000). However, in the tree shrew, laminae 1, 2, 4, and 5 all receive mixed projections comprised of both magnocellular and parvocellular input while laminae 3 and 6 are solely comprised of koniocellular input (Conway & Schiller, 1983; Conley, Fitzpatrick, & Diamond, 1984; Holdefer & Norton, 1995). Thus, magnocellular and parvocellular pathways overlap in geniculate laminae while the koniocellular pathway is segregated, which highlights the tree shrew species as a suitable model to study the koniocellular pathway in isolation.

The morphological properties of RGC axons terminating on geniculate relay cells are also extensively described: the primary excitatory synapses to LGN cells come from RGC axons. The retinal axons synapse onto geniculate relay cell dendrites via very large, glutamatergic axon terminals that are VGLUT2+ (Guillery, 1970; Kaas, Guillery, & Allman, 1972; Hamos, Van Horn, Raczkowski, & Sherman, 1987; Erisir, Horn, & Sherman, 1998; Van Horn et al., 2000; Sherman & Guillery, 2001; Land, Kyonka, & Shamalla-Hannah, 2004; Balaram, Takahata, & Kaas, 2011; Rovo, Ublert, & Acsady, 2012; Balaram, Isaamullah, Petry, Bickford, & Kaas, 2015). These retinal axons synapse on larger caliber dendrites and engage in triads, where geniculate inputs interact with one another on relay cell and interneuron dendrites to create complex synaptic arrangements (Famiglietti & Peters, 1972; Lieberman & Webster, 1974), termed triadic arrangements, and are known as ‘RLPs’ for their round vesicles, large

size, and pale mitochondria (Erisir et al., 1998; Li, Wang, & Bickford, 2003). The terminal cross-section areas and the relative contribution of input synapses to geniculate circuitry was studied extensively in the cat (Erisir, Van Horn, Bickford, & Sherman, 1997; Erisir, Van Horn, & Sherman, 1997; Erisir et al., 1998): corticothalamic axons have terminals that are the smallest in size, while cholinergic inputs are only slightly larger. Together, these two terminal populations make up ~60% of all LGN terminals (Erisir et al., 1997; Sherman & Guillery, 2001). GABAergic terminals, including interneuron and thalamic reticular nucleus (TRN) terminals, are medium in size and make up ~33% of LGN inputs (Sherman & Guillery, 2001). While retinal axons are the largest terminal boutons found in the LGN, they only provide 6% of synapses in the LGN (Sherman & Guillery, 2001). This complex, heterogenous geniculate circuitry suggests that there may be synaptic organization specific to different parallel pathways.

Given that the koniocellular parallel pathway is isolated and distinct from magno and parvo parallel pathways in tree shrews, I've chosen to conduct my experiments using this animal model. Tree shrews also serve as an advantageous animal model because of their LGN laminae organization and parallel pathway segregation. The organization of the tree shrew dLGN parallel pathways contains three pairs of layers (Holdefer & Norton, 1995): layers 1 and 2, layers 4 and 5, and layers 3 and 6 (Figure 2). Layers 1 and 2 form a pair that receives ipsilateral and contralateral projections, respectively, from medium to large-sized RGCs and display ON-center receptive field properties. Layers 4 and 5 form a pair that receives contralateral and ipsilateral projections, respectively, from medium to large-sized RGCs and display OFF-center receptive field properties. The only layers that receive input from the SC, laminae 3 and 6 (Diamond, Conley, Fitzpatrick, & Raczkowski, 1991; Figure 2), form a pair that receives contralateral projections from small-sized RGCs and display W-like (koniocellular) and ON-OFF center receptive field organization (Conway & Schiller, 1983; Holdefer & Norton, 1995).

Interestingly, many cells in koniocellular laminae show patterns of immunoreactivity that are distinct from that of parvocellular and magnocellular laminae (Hendry & Yoshioka, 1994; Goodchild & Martin, 1998; Hendry & Reid, 2000; Solomon, 2002; Casagrande & Xu, 2004). For example, histochemical studies have shown that laminae 1, 2, 4, and 5 stain more heavily for cytochrome oxidase in tree shrews (Wong-Riley & Norton, 1988). Additionally, calcium binding protein distributions are also differentiated by layer in the tree shrew: laminae 1, 2, 4, and 5 reveal parvalbumin reactivity while laminae 3 and 6 reveal calbindin reactivity (Diamond, Fitzpatrick, & Schmechel, 1993). These patterns reveal that the koniocellular pathway is a distinct part of the afferent visual stream in tree shrews with apparent differences from magno/parvo parallel pathways. There is also evidence that TG terminals, similar to RGC axons (Land et al., 2004), may use VGLUT2 for excitatory transmission. The evidence for this was provided in studies by Balaram et al., who showed that small, moderately labeled SC cells expressing VGLUT2 *mRNA* in the upper SGS corresponded to the cells that project to laminae 3 and 6 of the dLGN in both tree shrews (2011) and primates (2015). The evidence that TG projections in tree shrews may use VGLUT2 for excitatory transmission, in conjunction with the aforementioned benefits, supports the decision that the tree shrew is the most advantageous animal model to study this parallel pathway channel segregation.

Based on this accumulated knowledge on organization of parallel pathways and the TG inputs to LGN, I addressed the following hypotheses in this study:

Hypothesis 1: <u>The synaptic circuitries formed by magno/parvo and koniocellular RGC terminals are not uniform.</u> I tested this hypothesis by analyzing the morphological properties of VGLUT2+ and unlabeled terminals, synapses and their postsynaptic partners in geniculate lamina that receive exclusively koniocellular input in comparison to those that receive magno- and parvocellular axons. The differences in terminal bouton size and the types of postsynaptic

sites in each lamina examined revealed that VGLUT2+ magno and parvo RGC terminals are remarkably different than the VGLUT2+ excitatory terminals in the koniocellular lamina. The evidence supporting non-uniform circuitries suggests that the information carried through the relay cells to cortex are being regulated differentially in these parallel pathways.

Hypothesis 2: The synaptic circuitries formed by RGC or TG axons are not uniform. I tested this hypothesis by analyzing the morphological properties of VGLUT2+ terminals in lamina 6, one of the TG-recipient layers in the tree shrew dLGN. The non-uniform clustering of terminal morphology and synaptic connectivity parameters suggested that there is more than one VGLUT2+ input, and that these two inputs may have different properties in exciting the koniocellular relay cells. Second, I characterized the morphological properties of TG terminals alone using anterograde tract-tracing. The comparison of the TG terminals to VGLUT2+ terminals in the koniocellular layers confirmed the unique properties of koniocellular RGC versus the TG terminals in the LGN.

Materials and Methods

Animals

Data for this study was collected from the brains of three adult tree shrews (*Tupaia belangeri*) of both sexes. All procedures in this study were approved by the University of Virginia Institutional Animal Care and Use Committee (IACUC).

Biotinylated dextran amine injections

In order to label tectogeniculate (TG) projections via anterograde transport, adult tree shrews were anesthetized with isoflurane and placed in a stereotaxic apparatus. An incision was made along the scalp and a small hole was drilled in the skull above the SC. A glass pipette containing a 5% solution of biotinylated dextran amine (BDA; Invitrogen) in saline was

lowered into the SC. After removal of the pipette, the scalp skin was sealed with a tissue adhesive and animals were placed on a heating pad until mobile. After surgery, animals were carefully monitored for seven days to ensure proper wound healing and were observed for any behaviors indicative of pain or discomfort.

Tissue preparation

After 14 days required for tracer transport from SC to LGN, the animals were deeply anesthetized with an overdose of euthasol (excess of 0.25mL/kg i.p.) and transcardially perfused with Tyrode's solution followed by 300mL of fixative solution containing 4% paraformaldehyde (PF), and 0.5% or 2% glutaraldehyde in 0.1M phosphate buffer (pH 7.4). Brains were extracted and post-fixed overnight in 4% PF at 4°C. Brains were then blocked and sectioned at 60µm on a vibratome in a series of four. One series (#4) was mounted on subbed slides for histochemical stains. One of the series was set aside for resin embedding for EM analysis. All other sections were rinsed in 1% sodium borohydride and stored in 0.05% sodium azide in 0.01M PBS at 4°C prior to immunohistochemistry.

Histochemistry

For myelin visualization, sections that were mounted on subbed slides were rehydrated in 0.02M PBS for 2 minutes and incubated in 0.2% gold chloride ($HAuCl_4$) for 12-15 minutes at 60°C. Once fine myelinated fibers were differentiated, the slides were transferred in an intensification solution of 0.2% potassium gold chloride ($KauCl_4$) for 2-3 minutes at 60°C, followed by two rinses in 0.02m PBS for 2 minutes each. Finally, sections were incubated in 1% sodium thiosulfate ($Na_2O_3S_2$) for 3 minutes at 60°C, followed by 3 rinses in 0.02M PBS for 3 minutes each. The slides were then treated through a series of ETOH for dehydration and xylenes for clearing the tissue of lipids. All slides were coverslipped using DPX mounting media (Sigma Aldrich, St. Louis, MO).

Immunohistochemistry

Antibodies: Terminals positive for vesicular glutamate transporter type 2 (VGLUT2) were identified with guinea pig polyclonal anti-VGLUT2 (EMD Millipore, Burlington, MA). Details for primary and secondary antibodies are described in Table 1.

Pre-embedding immunostaining: Sections were pre-incubated in 1% BSA in 0.01M PB with 0.06% Triton-X and 0.05% sodium azide (NaN_3) for 30 minutes. Sections were then transferred into primary antibody anti-VGLUT2 in 1% BSA-PBS and 0.05% sodium azide for 72h on a shaker. To terminate the incubation, sections were rinsed in 0.01M PBS before being transferred to a secondary antibody conjugated to biotin for 2h. This was followed by a treatment avidin-biotin-complex (ABC; Vector) solution for 2h. Sections were then rinsed in 0.01M PBS and incubated in a solution of hydrogen peroxide (H_2O_2) and 0.05% diaminobenzidine (DAB) for 2-7 minutes.

Embedding for electron microscopy

Sections were treated with 1% osmium tetroxide (OsO_4) in 0.1M PB for one hour. Sections were then treated with filtered 4% uranyl acetate in 70% alcohol for one hour, followed by dehydration in acetone and treatment with a 1:1 acetone/resin mixture overnight. The following day, sections were transferred to full resin and left overnight. Sections were then flat embedded between two aclar sheets and were cured in a 60°C oven overnight. Sections of LGN to be used for EM were identified from flat embed sections and photographed with a light microscope. The region of interest from each section, containing LGN, were placed in BEEM capsules (EMS, Hatfield, PA). The capsules were filled with resin and cured at 60°C for 24-48 hours, or until polymerized. The region of interest (now capsule embedded) was traced with a camera lucida and trimmed down to a 1mm x 2mm trapezoid containing the entirety of LGN (Figure 3a,b). Ultrathin sections of ~50-80nm thickness were collected on 400 mesh copper

grids (Ted Pella, Redding, CA) using an ultramicrotome (Ultracut UCT7; Leica, Buffalo Grove, IL). The orientation of the trapezoid could be seen at lower magnification in the electron microscope so that we could locate which end would contain tissue from a particular lamina (Figure 3c).

Imaging and Analysis

To obtain images for light microscopy figures, sections were photographed using a Leica microscope (Model LMDC 888011) and Leica MC170 digital camera. Photographs were annotated using Adobe Photoshop software.

For electron microscopy (EM) images, ultrathin sections on copper grids were examined on a JEOL1010 electron microscope equipped with a 16-megapixel CCD camera (SIA). Images for quantitative morphology and immuno-labeled terminal analysis were taken at 12kX-15kX magnification, yielding a resolution of 907.47-1134.92 pixels/μm. For analysis, overlapping EM images were captured and stitched to create composite areas across the layers of the dLGN. Fiji ImageJ (Media Cybernetics, Silver Spring, MD) was used to quantify terminal area and synapse length. Both unlabeled and labeled terminals were outlined to obtain their area, while synapses were traced to obtain their length.

The statistical analysis for nonparametric testing, including Mann-Whitney U tests and descriptive statistics, was performed using GraphPad Prism software (GraphPad.com). Multimodal distribution analysis for terminal size was conducted using the MClust package in R (version 3.6.2). All figures and graphs were created using Prism, RStudio, Procreate, and Adobe Photoshop.

Results

VGLUT2 Terminals in Koniocellular and Magno/Parvo Geniculate Laminae

While geniculate laminae 1, 2, 4, and 5 receive synaptic input from parvocellular (X-type) and magnocellular (Y-type) retinal ganglion cells (RGCs), laminae 3 and 6 receive koniocellular (W-type) input. In order to identify if the morphological and connective properties of VGLUT2 terminals in koniocellular geniculate laminae differ from those in magno/parvo type laminae, I have examined synaptic terminals in lamina 6 (koniocellular) and laminae 1-2 (magno/parvo).

Qualitative properties of VGLUT2 terminals: In all geniculate laminae, VGLUT2 immunostaining led to dense DAB accumulation (Figure 4) at the light microscopy resolutions. The geniculate laminae 1-6 display particularly dense puncta, while interlaminar regions show sparse or no labeling with VGLUT2 (Figure 4a-c).

At the electron microscopy resolution, VGLUT2+ terminals in the geniculate laminae are evident by the diffusely dark labeling in vesicle-filled cross-sections. These labeled synaptic terminals contained many round vesicles and typically many mitochondria (Figure 5). The majority of VGLUT2+ terminals contain mitochondria, however, whether or not the mitochondria are pale could not be ascertained due to the dark DAB labeling that surrounds these organelles. Pale mitochondria are specific to and characteristic of RGCs and their axons. The labeled terminals often displayed unlabeled, membrane bound inclusions which are often observed as emerging from dendrites (Figure 5a). These unlabeled patches, or 'protrusions', can be postsynaptic to the terminals. The labeled terminals also formed synapses on dendritic shafts of various calibers. Synapses formed by these terminals displayed a thick, dark postsynaptic density. Unlabeled terminals showed a range of morphological properties, with some having more sparse vesicles and little to no mitochondria, and also formed synapses on dendritic shafts of various calibers.

Quantitative properties of VGLUT2+ terminals: Pairs of geniculate laminae in tree shrew LGN represent different parallel pathways: while laminae 1, 2, 4, and 5 receive axons from magnocellular and parvocellular RGCs, laminae 3 and 6 receive koniocellular input. Furthermore, while the VGLUT2+ terminals in 1, 2, 4 and 5 arise only from the RGC axons,

those in laminae 3 and 6 may come from both the retina and SC. In order to characterize any morphological differences among the magno/parvo vs. koniocellular axon terminals, I compared the terminal cross-section areas in geniculate laminae 1-2 and lamina 6. I use *terminal cross-section area* as a measure of terminal bouton size, which may display RGC-type dependent morphometric properties. For this, I captured at least 500 slightly overlapping EM images at 12kX magnification, from the tree shrew dLGN laminae 1-2 and lamina 6. The pixel size of the images were 907.473 pixels/μm, yielding sufficient resolution to differentiate two layers of the lipid bilayers. The images were examined using Fiji ImageJ. Every terminal (labeled or unlabeled) that displayed a synapse at the cross section was marked and measured, yielding a final data set that included 276 terminals. In a sample of 89 VGLUT2+ terminals, the terminal sizes ranged between 0.142 μm^2 and 5.093 μm^2. The average cross-sectional area of VGLUT2+ terminals in laminae 1 and 2 was 1.93 μm^2 ± 1.05 μm^2, ranging between 0.260 μm^2 and 5.093 μm^2 (Figure 6c). The average cross-sectional area of VGLUT2+ terminals in lamina 6 was 0.70 μm^2 ± 0.57 μm^2, ranging between 0.142 μm^2 and 3.499 μm^2 (Figure 6d) and displaying a multimodal distribution formed by at least 2 distinct populations (Figure 6e). VGLUT2+ terminals in laminae 1 and 2 are statistically larger than the VGLUT2+ terminals in lamina 6 (Mann-Whitney U test, $p < .0001$; Figure 6b). I also measured the terminal cross-sectional area of terminals that appeared in the same images but were not positive for VGLUT2. The VGLUT2-unlabeled terminal sizes ranged between 0.071 μm^2 and 2.314 μm^2 (mean = 0.43 μm^2). In both laminae 1-2 and lamina 6, the VGLUT2+ terminals were statistically larger than the VGLUT2-unlabeled terminal populations (Mann-Whitney U test, $p < .0001$; Figure 6a).

Targeting properties of VGLUT2+ terminals: In order to reveal whether the circuitries formed by VGLUT2+ terminals in laminae 1-2 and lamina 6 are similar or display pathway-specific properties, I also analyzed the selectivity of terminals to different compartments of the postsynaptic cells. For every labeled terminal collected, I identified the postsynaptic target of each synapse as a dendrite shaft, a protrusion, or a vesicle-filled profile. Synapsing on a

vesicle-filled profile is a property of retinal terminals, yielding triadic and glomerular arrangements. I particularly asked whether the targeting properties of VGLUT2+ terminals in koniocellular geniculate laminae differ from those in magno/parvo type laminae. The majority of VGLUT2+ terminals in laminae 1 and 2 synapsed onto dendritic shafts and targeted vesicle-filled profiles the least (Table 2). For VGLUT2+ terminals collected from lamina 6, the majority of terminals synapsed onto vesicle-filled profiles and targeted protrusions the least (Table 2).

For every labeled terminal collected, I also identified various morphological properties, including presence of protrusions, involvement in triadic arrangements, and number of synapses. The majority of VGLUT2+ terminals in laminae 1 and 2 contained protrusions, while only one-fifth of VGLUT2+ terminals in lamina 6 contained protrusions (Table 3). More VGLUT2+ terminals were involved in triadic arrangements in lamina 6 versus in laminae 1 and 2 (Table 3). For VGLUT2+ terminals collected from laminae 1 and 2, the majority of terminals made only 1 synapse, but many terminals made multiple synaptic contacts (Table 3). For VGLUT2+ terminals collected from lamina 6, a large majority of terminals made only 1 synapse, but there were very few terminals that made multiple synaptic contacts (Table 3).

Superior Colliculus Terminals in Laminae 3 and 6 of dLGN

Qualitative properties of tectogeniculate terminals: In laminae 3 and 6, terminals anterogradely labeled with BDA are densely filled with dark chromogen of DAB, round vesicles, and little to no mitochondria (Figure 7). The labeled terminals also formed synapses on dendritic shafts of various calibers. Synapses formed by these terminals displayed a thick, dark postsynaptic density.

Quantitative properties of tectogeniculate terminals: The measurements of terminal bouton cross-sectional area can be used to differentiate distinct inputs to the thalamus (Guillery, 1969; Erisir et al., 1997; Van Horn, Erisir, & Sherman, 2000). To determine the quantitative distribution of terminal bouton sizes, in order to distinguish if TG inputs have a distinct terminal

size, the size distribution of terminal cross-sectional areas were analyzed. For this analysis, I collected images of each identified labeled terminal in laminae 3 or 6 of dLGN at 12kX-15kX magnification with a pixel size of 907.473-1134.917 pixels/μm. I also collected images in the surrounding area of the labeled terminal to collect data for unlabeled terminals. These images were examined using Fiji ImageJ, where every terminal that displayed a synapse at the cross section was marked and measured, yielding a final data set that included 47 terminals. In a sample of 18 BDA-labeled terminals, the average cross-sectional area of terminals was 0.30 $\mu m^2 \pm 0.08\ \mu m^2$, ranging between 0.155 μm^2 and 0.413 μm^2. VGLUT2+ terminal areas in laminae 1 and 2 are significantly different from BDA-labeled terminal areas (Mann-Whitney U test, $p < .0001$, Figure 8a). VGLUT2+ terminal areas in lamina 6 are significantly different from BDA-labeled terminal areas (Mann-Whitney U test, $p < .0001$; Figure 8c). I also measured the terminal cross-sectional area of terminals that appeared in the same images but were not labeled with BDA. The BDA-unlabeled terminal sizes ranged between 0.116 μm^2 and 1.989 μm^2 (mean = 0.42 μm^2). BDA-labeled terminals are not significantly different from BDA-unlabeled terminal populations (Figure 8b).

Targeting properties of TG terminals: For every BDA-labeled terminal collected, I identified the postsynaptic target of each synapse as a dendrite shaft, a protrusion, or a vesicle-filled profile. Synapsing on a vesicle-filled profile is a property of retinal terminals, yielding triadic and glomerular arrangements. I particularly asked whether the targeting properties of TG terminals differ from retinal terminals. The majority of BDA-labeled terminals synapsed onto dendritic shafts and targeted protrusions the least (Table 2).

For every labeled terminal collected, I also identified various morphological properties, including presence of protrusions, involvement in triadic arrangements, and number of synapses. There were not any TG terminals that contained protrusions and a small percentage of BDA-labeled terminals were engaged in triadic arrangements (Table 3). Every BDA-labeled terminal collected made only 1 synapse (Table 3).

Discussion

The current study characterized the morphological and synaptic properties of VGLUT2+ and TG terminals in dLGN laminae. VGLUT2+ terminals in koniocellular (W-type) laminae, which receive input from the SC, were compared to VGLUT2+ terminals in parvocellular (X-type)/magnocellular (Y-type) laminae, which do not receive input from the SC. VGLUT2+ terminals in koniocellular lamina 6 were also compared to TG terminals. This study provided evidence that VGLUT2+ terminals in koniocellular laminae differ, both in their morphology and synaptic properties, from magno/parvo laminae (Figure 9). VGLUT2+ terminals in lamina 6 were smaller, had less visible protrusions, made less synaptic contacts, and engaged in more triadic arrangements than VGLUT2+ terminals in laminae 1 and 2. Additionally, VGLUT2+ terminals in lamina 6 revealed a multimodal distribution consisting of two distinct subpopulations of terminal sizes. Comparison of terminal area distributions between BDA-labeled and VGLUT2+ terminals in lamina 6 suggest that TG terminals could constitute the smaller terminal size subpopulation in koniocellular laminae.

Ultrastructure morphology of tree shrew dLGN

In the visual thalamus, the input axons from the retina bring the largest terminal boutons found in dLGN (Erisir et al., 1998; Van Horn et al., 2000; Cavdar, Hacıoğlu, Keskinöz, & Onat, 2011). These large terminals also constitute the VGLUT2 immunoreactive population (Fremeau Jr. et al., 2001; Varoqui, Schäfer, Zhu, Weihe, & Erickson 2002; Land et al., 2004; Rovo et al., 2012) that tend to make multiple synaptic zones, synapse onto more proximal dendrites, and engage in triadic arrangements (Hamos et al., 1987; Montero, 1991; Cavdar et al., 2011; Rovo et al., 2012). This primary retinal input is named RLP for its round vesicles, large profile, and pale mitochondria (Erisir et al., 1998). The large-sized terminal population found in laminae 1, 2, and 6 displayed the morphological characteristics that we would anticipate seeing in RLPs, such

as large VGLUT2+ boutons, many large mitochondria, and asymmetric synapses. The frequency distribution histograms of terminal bouton area in VGLUT2-immunostained tissue revealed that, as anticipated, VGLUT2+ terminals are the largest terminals in dLGN laminae. Although VGLUT2+ terminals in lamina 6 were larger than their respective unlabeled population, these terminals were still significantly smaller than VGLUT2+ terminals in laminae 1 and 2. VGLUT2+ terminals in koniocellular lamina 6 had a multimodal population of small and large terminal size subpopulations, indicating that there may be more than one type of origin for these terminals. While lamina 6 still contained large, labeled terminals that resembled RLPs, I also observed smaller labeled terminals with very few mitochondria and no protrusions that were similar to the morphological characteristics of TG terminals. Additionally, when comparing the terminal area distributions of BDA-labeled and VGLUT2+ terminals in lamina 6, it appears that TG terminals could constitute the smaller sized subpopulation since the VGLUT2+ terminals in lamina 6 were significantly larger than the BDA-labeled terminals. Overall, the non-homogenous VGLUT2+ terminal population in laminae that receive input from the SC suggests that TG projections may be the smaller terminal size subpopulation of VGLUT2+ terminals in lamina 6.

VGLUT2+ terminals in koniocellular laminae differ from those in magno/parvo laminae

Retinal terminals, or RLPs, have several characteristics that are specific to their terminal morphology and driving input, including the presence of protrusions, engagement in triadic arrangements, and making multiple synapses (Hamos et al., 1987; Montero, 1991; Erisir et al., 1998; Cavdar et al., 2011; Rovo et al., 2012). If the VGLUT2+ terminals in koniocellular lamina 6 are non-homogenous, we would anticipate that their synaptic properties would differ from VGLUT2+ terminals in magno/parvo laminae.

It was found that VGLUT2+ terminals in laminae 1 and 2 were most likely to target dendritic shafts and least likely to target vesicle-filled profiles. Contrastingly, VGLUT2+ terminals in lamina 6 were most likely to target vesicle-filled profiles and least likely to target protrusions.

These preferential targets reveal robust large terminals that are projecting to magno/parvo laminae and contacting dendrite shafts more than protrusions or vesicle-filled profiles, which may be a unique population to only magno/parvo laminae. There was also a higher percentage of VGLUT2+ terminals that contained protrusions in laminae 1 and 2 than in lamina 6. Additionally, there was a higher percentage of VGLUT2+ terminals making only 1 synapse in lamina 6, while a higher percentage of VGLUT2+ terminals made more than 1 synapse in laminae 1 and 2 (notably, there were no VGLUT2+ terminals in lamina 6 that made more than 3 synapses). Overall, morphological and synaptic characteristics of RLPs appeared more in laminae that only receive retinal input than in laminae that receive input from both the retina and SC. Interestingly, there was a higher percentage of VGLUT2+ terminals involved in triadic arrangements in lamina 6. Since we cannot, with certainty, state whether it was an RLP or TG terminal involved in the triads, future studies (discussed below) will be performed to determine if TG terminals have a higher preference for interneurons. However, the majority of BDA-labeled terminals collected were not involved in triadic arrangements, suggesting that triads may be a feature of the koniocellular pathway retinal axons. Overall, these findings support the hypothesis that synaptic properties differ in koniocellular versus magno/parvo laminae. Given that, overall, VGLUT2+ terminals in lamina 6 had a higher percentage of properties that are uncharacteristic of RLPs, it further suggests that TG terminals could be responsible for this difference.

Limitations and Future Directions

These results serve as an important first step in uncovering differences in these parallel pathways and determining how the SC may be involved in this visual thalamic network. However, there are some limitations to this study, primarily due to the small sample size of the BDA population (for both unlabeled and labeled terminals). Further data will need to be collected before addressing the hypothesis that TG terminals have different synaptic properties

from retinal terminals. Nonetheless, there is strong evidence in support of a non-homogenous VGLUT2+ population across dLGN laminae. In order to further ascertain the morphological and synaptic properties of TG projections in the tree shrew visual system, we will complete the following studies:

1. *Dual injections to analyze interactions between TG and retinal terminals.* Cholera toxin subunit B will be injected into the retina and will label the cytoplasm of retinal terminals while a Ginty virus, which targets peroxidase reporters to distinct cellular compartments, will be injected into the SC to label the organelles of TG terminals. This will allow us to distinguish SC projections from retinal terminals and potentially visualize both a TG and retinal terminal interacting on the same dendrite so that we can start to learn how these inputs are interacting in the LGN.
2. *Calbindin staining and post-embedding immunogold labeling to determine targeting properties for interneurons.* An interesting observation is that calcium binding protein distributions are differentiated by layer in the tree shrew dLGN, with layers 1, 2, 4, and 5 showing parvalbumin reactivity and layers 3 and 6 showing calbindin reactivity (Diamond et al., 1993). Post-embedding immunogold labeling identifies GABA-containing profiles and will allow us to distinguish between profiles of relay cells and interneurons and then determine the distribution of terminal types making contact onto relay cells and interneurons. Given previous differences found in immunoreactivity in koniocellular versus magno/parvo parallel pathways, along with the finding that VGLUT2+ terminals in lamina 6 engage in more triadic arrangements, these methods would help determine if SC terminals have a higher preference for interneurons, which could, in turn, provide further insight into the SC's role in mediating relay cell information in koniocellular laminae.

References

Albano, J. E., Norton, T. T., & Hall, W. C. (1979). Laminar origin of projections from the superficial layers of the superior colliculus in the tree shrew, Tupaia glis. *Brain research*, *173*(1), 1-11.

Balaram, P., Takahata, T., & Kaas, J. H. (2011). VGLUT2 mRNA and protein expression in the visual thalamus and midbrain of prosimian galagos (Otolemur garnetti). *Eye and brain*, *3*, 5.

Balaram, P., Isaamullah, M., Petry, H. M., Bickford, M. E., & Kaas, J. H. (2015). Distributions of vesicular glutamate transporters 1 and 2 in the visual system of tree shrews (Tupaia belangeri). *Journal of Comparative Neurology*, *523*(12), 1792-1808.

Basso, M. A., & Wurtz, R. H. (1998). Modulation of neuronal activity in superior colliculus by changes in target probability. *Journal of Neuroscience*, *18*(18), 7519-7534.

Benevento, L. A., & Standage, G. P. (1983). The organization of projections of the retinorecipient and nonretinorecipient nuclei of the pretectal complex and layers of the superior colliculus to the lateral pulvinar and medial pulvinar in the macaque monkey. *Journal of Comparative Neurology*, *217*(3), 307-336.

Bickford, M. E., Zhou, N., Krahe, T. E., Govindaiah, G., & Guido, W. (2015). Retinal and tectal "driver-like" inputs converge in the shell of the mouse dorsal lateral geniculate nucleus. *Journal of Neuroscience*, *35*(29), 10523-10534.

Boycott, B. B., & Wässle, H. (1974). The morphological types of ganglion cells of the domestic cat's retina. *The Journal of physiology*, *240*(2), 397-419.

Campbell, C. B. G., Jane, J. A., & Yashon, D. (1967). The retinal projections of the tree shrew and hedgehog. *Brain Research*, *5*(3), 406-418.

Casagrande, V. A. (1991). Lateral geniculate nucleus: a review of its physiology and function. *The neural basis of visual function*, *4*, 41-84.

Casagrande, V. A. (1994). A third parallel visual pathway to primate area V1. *Trends in neurosciences*, *17*(7), 305-310.

Casagrande, V. A., & Xu, X. (2004). 31 Parallel Visual Pathways: A Comparative Perspective.

Çavdar, S., Hacıoğlu, H., Şirvancı, S., Keskinöz, E., & Onat, F. (2011). Synaptic organization of the rat thalamus: a quantitative study. *Neurological Sciences*, *32*(6), 1047-1056.

Conley, M., Fitzpatrick, D., & Diamond, I. T. (1984). The laminar organization of the lateral geniculate body and the striate cortex in the tree shrew (Tupaia glis). *Journal of Neuroscience*, *4*(1), 171-197.

Conway, J. L., & Schiller, P. H. (1983). Laminar organization of tree shrew dorsal lateral geniculate nucleus. *Journal of neurophysiology*, *50*(6), 1330-1342.

Dacey, D. M., & Petersen, M. R. (1992). Dendritic field size and morphology of midget and parasol ganglion cells of the human retina. *Proceedings of the National Academy of sciences*, *89*(20), 9666-9670.

Diamond, I. T., Conley, M., Fitzpatrick, D., & Raczkowski, D. (1991). Evidence for separate pathways within the tecto-geniculate projection in the tree shrew. *Proceedings of the National Academy of Sciences*, *88*(4), 1315-1319.

Diamond, I. T., Fitzpatrick, D., & Schmechel, D. (1993). Calcium binding proteins distinguish large and small cells of the ventral posterior and lateral geniculate nuclei of the prosimian galago and the tree shrew (Tupaia belangeri). *Proceedings of the National Academy of Sciences*, *90*(4), 1425-1429.

Druga, R., & Syka, J. (1984). Projections from auditory structures to the superior colliculus in the rat. *Neuroscience letters*, *45*(3), 247-252.

Edwards, S. B., Ginsburgh, C. L., Henkel, C. K., & Stein, B. E. (1979). Sources of subcortical projections to the superior colliculus in the cat. *Journal of Comparative Neurology*, *184*(2), 309-329.

Erişir, A., Van Horn, S. C., Bickford, M. E., & Sherman, S. M. (1997). Immunocytochemistry and distribution of parabrachial terminals in the lateral geniculate nucleus of the cat: a comparison with corticogeniculate terminals. *Journal of Comparative Neurology*, *377*(4), 535-549.

Erişir, A., Van Horn, S. C., & Sherman, S. M. (1997). Relative numbers of cortical and brainstem inputs to the lateral geniculate nucleus. *Proceedings of the National Academy of Sciences*, *94*(4), 1517-1520.

Erişir, A., Van Horn, S. C., & Sherman, S. M. (1998). Distribution of synapses in the lateral geniculate nucleus of the cat: differences between laminae A and A1 and between relay cells and interneurons. *Journal of Comparative Neurology*, *390*(2), 247-255.

Famiglietti Jr., E. V., & Peters, A. (1972). The synaptic glomerulus and the intrinsic neuron in the dorsal lateral geniculate nucleus of the cat. *Journal of Comparative Neurology*, *144*(3), 285-333.

Feig, S., & Harting, J. K. (1992). Ultrastructural studies of the primate parabigeminal nucleus: electron microscopic autoradiographic analysis of the tectoparabigeminal projection in Galago crasssicaudatus, *Brain Research*, *595*(2), 334-338.

Fitzpatrick, D., Conley, M., Luppino, G., Matelli, M., & Diamond, I. T. (1988). Cholinergic projections from the midbrain reticular formation and the parabigeminal nucleus to the lateral geniculate nucleus in the tree shrew. *Journal of Comparative Neurology*, *272*(1), 43-67.

Fremeau Jr., R. T., Troyer, M. D., Pahner, I., Nygaard, G. O., Tran, C. H., Reimer, R. J., ... & Edwards, R. H. (2001). The expression of vesicular glutamate transporters defines two classes of excitatory synapse. *Neuron*, *31*(2), 247-260.

Goodchild, A. K., & Martin, P. R. (1998). The distribution of calcium-binding proteins in the lateral geniculate nucleus and visual cortex of a New World monkey, the marmoset, Callithrix jacchus. *Visual Neuroscience*, *15*(4), 625-642.

Graham, J., & Casagrande, V. A. (1980). A light microscopic and electron microscopic study of the superficial layers of the superior colliculus of the tree shrew (Tupaia glis). *Journal of Comparative Neurology*, *191*(1), 133-151.

Grantyn, A., & Grantyn, R. (1982). Axonal patterns and sites of termination of cat superior colliculus neurons projecting in the tecto-bulbo-spinal tract. *Experimental Brain Research*, *46*(2), 243-256.

Graybiel, A. M. (1975). Anatomical organization of retinotectal afferents in the cat: An autoradiographic study. *Brain research*, *96*(1), 1-23.

Graybiel, A. M. (1978). A satellite system of the superior colliculus: the parabigeminal nucleus and its projections to the superficial collicular layers. *Brain research*, *145*(2), 365-374.

Güillery, R. W. (1969). A quantitative study of synaptic interconnections in the dorsal lateral geniculate nucleus of the cat. *Zeitschrift für Zellforschung und mikroskopische Anatomie*, *96*(1), 39-48.

Guillery, R. W. (1970). The laminar distribution of retinal fibers in the dorsal lateral geniculate nucleus of the cat: a new interpretation. *Journal of Comparative Neurology*, *138*(3), 339-367.

Hall, W. C., Fitzpatrick, D., Klatt, L. L., & Raczkowski, D. (1989). Cholinergic innervation of the superior colliculus in the cat. *Journal of Comparative Neurology*, *287*(4), 495-514.

Hamos, J. E., Van Horn, S. C., Raczkowski, D., & Sherman, S. M. (1987). Synaptic circuits involving an individual retinogeniculate axon in the cat. *Journal of Comparative Neurology*, *259*(2), 165-192.

Harting, J. K., Huerta, M. F., Hashikawa, T., & van Lieshout, D. P. (1991). Projection of the mammalian superior colliculus upon the dorsal lateral geniculate nucleus: organization of tectogeniculate pathways in nineteen species. *Journal of Comparative Neurology*, *304*(2), 275-306.

Harting, J. K., Updyke, B. V., & van Lieshout, D. P. (1992). Corticotectal projections in the cat: Anterograde transport studies of twenty-five cortical areas. *Journal of Comparative Neurology*, *324*(3), 379-414.

Hendry, S. H., & Reid, R. C. (2000). The koniocellular pathway in primate vision. *Annual review of neuroscience*, *23*(1), 127-153.

Hendry, S. H., & Yoshioka, T. (1994). A neurochemically distinct third channel in the macaque dorsal lateral geniculate nucleus. *Science*, *264*(5158), 575-577.

Holdefer, R. N., & Norton, T. T. (1995). Laminar organization of receptive field properties in the dorsal lateral geniculate nucleus of the tree shrew (*Tupaiaglis belangeri*). *Journal of comparative neurology*, *358*(3), 401-413.

Horwitz, G. D., Batista, A. P., & Newsome, W. T. (2004). Representation of an abstract perceptual decision in macaque superior colliculus. *Journal of neurophysiology*, *91*(5), 2281-2296.

Huerta, M. F., Weber, J. T., Rothstein, L. R., & Harting, J. K. (1985). Subcortical connections of area 17 in the tree shrew: an autoradiographic analysis. *Brain research*, *340*(1), 163-170.

Jiang, Z. D., Moore, D. R., & King, A. J. (1997). Sources of subcortical projections to the superior colliculus in the ferret. *Brain research*, *755*(2), 279-292.

Kaas, J. H., Guillery, R. W., & Allman, J. M. (1972). Some Principles of Organization in the Dorsal Lateral Geniculate Nucleus; pp. 283–299. *Brain, Behavior and Evolution*, *6*(1-6), 283-299.

Kaas, J. H., Huerta, M. F., Weber, J. T., & Harting, J. K. (1978). Patterns of retinal terminations and laminar organization of the lateral geniculate nucleus of primates. *Journal of Comparative Neurology*, *182*(3), 517-553.

Kaplan, E. (2004). The M, P, and K pathways of the primate visual system. *The visual neurosciences*, *1*, 481-493.

Kaplan, E. (2014). The M, P and K pathways of the primate visual system revisited. *The new visual neurosciences (Werner JS, Chalupa LM, eds.). Cambridge, MA: Massachusetts Institute of Technology*.

Kerschensteiner, D., & Guido, W. (2017). Organization of the dorsal lateral geniculate nucleus in the mouse. *Visual neuroscience*, *34*.

Lachica, E. A., & Casagrande, V. A. (1993). The morphology of collicular and retinal axons ending on small relay (W-like) cells of the primate lateral geniculate nucleus. *Visual neuroscience*, *10*(3), 403-418.

Land, P. W., Kyonka, E., & Shamalla-Hannah, L. (2004). Vesicular glutamate transporters in the lateral geniculate nucleus: expression of VGLUT2 by retinal terminals. *Brain research*, *996*(2), 251-254.

Leventhal, A. G., Rodieck, R. W., & Dreher, B. (1981). Retinal ganglion cell classes in the Old World monkey: morphology and central projections. *Science*, *213*(4512), 1139-1142.

Li, J., Wang, S., & Bickford, M. E. (2003). Comparison of the ultrastructure of cortical and retinal terminals in the rat dorsal lateral geniculate and lateral posterior nuclei. *Journal of Comparative Neurology*, *460*(3), 394-409.

Li, X., & Basso, M. A. (2005). Competitive stimulus interactions within single response fields of superior colliculus neurons. *Journal of Neuroscience*, *25*(49), 11357-11373.

Li, X., & Basso, M. A. (2008). Preparing to move increases the sensitivity of superior colliculus neurons. *Journal of Neuroscience*, *28*(17), 4561-4577.

Lieberman, A. R., & Webster, K. E. (1974). Aspects of the synaptic organization of intrinsic neurons in the dorsal lateral geniculate nucleus. *Journal of neurocytology*, *3*(6), 677-710.

Lo, C. C., & Wang, X. J. (2006). Cortico–basal ganglia circuit mechanism for a decision threshold in reaction time tasks. *Nature neuroscience*, *9*(7), 956-963.

Lovejoy, L. P., & Krauzlis, R. J. (2010). Inactivation of primate superior colliculus impairs covert selection of signals for perceptual judgments. *Nature neuroscience*, *13*(2), 261-266.

Lui, F., Gregory, K. M., Blanks, R. H., & Giolli, R. A. (1995). Projections from visual areas of the cerebral cortex to pretectal nuclear complex, terminal accessory optic nuclei, and superior colliculus in macaque monkey. *Journal of Comparative Neurology*, *363*(3), 439-460.

Lund, R. D., Land, P. W., & Boles, J. (1980). Normal and abnormal uncrossed retinotectal pathways in rats: an HRP study in adults. *Journal of Comparative Neurology*, *189*(4), 711-720.

May, P. J. (2006). The mammalian superior colliculus: laminar structure and connections. *Progress in brain research*, *151*, 321-378.

Montero, V. M. (1991). A quantitative study of synaptic contacts on interneurons and relay cells of the cat lateral geniculate nucleus. *Experimental Brain Research*, *86*(2), 257-270.

Peichl, L. (1991). Alpha ganglion cells in mammalian retinae: common properties, species differences, and some comments on other ganglion cells. *Visual neuroscience*, *7*(1-2), 155-169.

Peichl, L., Ott, H., & Boycott, B. B. (1987). Alpha ganglion cells in mammalian retinae. *Proceedings of the Royal society of London. Series B. Biological sciences*, *231*(1263), 169-197.

Perry, V. H., Oehler, R., & Cowey, A. (1984). Retinal ganglion cells that project to the dorsal lateral geniculate nucleus in the macaque monkey. *Neuroscience*, *12*(4), 1101-1123.

Petry, H. M., Agarwala, S., & May III, J. G. (1989). Striped pattern of labeling in ground squirrel superior colliculus following intraocular HRP injections. *Brain research*, *489*(1), 199-203.

Pollack, J. G., & Hickey, T. L. (1979). The distribution of retino-collicular axon terminals in rhesus monkey. *Journal of Comparative Neurology*, *185*(4), 587-602.

Rodieck, R., & Watanabe, M. (1993). Survey of the morphology of macaque retinal ganglion cells that project to the pretectum, superior colliculus, and parvicellular laminae of the lateral geniculate nucleus. *Journal of Comparative Neurology*, *338*(2), 289-303.

Rovó, Z., Ulbert, I., & Acsády, L. (2012). Drivers of the primate thalamus. *Journal of Neuroscience*, *32*(49), 17894-17908.

Sherman, S. M., & Guillery, R. W. (2001). *Exploring the thalamus*. Elsevier.

Solomon, S. G. (2002). Striate cortex in dichromatic and trichromatic marmosets: neurochemical compartmentalization and geniculate input. *Journal of Comparative Neurology*, *450*(4), 366-381.

Sparks, D. L., & Hartwich-Young, R. (1989). The deep layers of the superior colliculus. *Rev Oculomot Res*, *3*, 213-255.

Stanford, L. R., Friedlander, M. J., & Sherman, S. M. (1981). Morphology of physiologically identified W-cells in the C laminae of the cat's lateral geniculate nucleus. *Journal of Neuroscience*, *1*(6), 578-584.

Tokuoka, K., Kasai, M., Kobayashi, K., & Isa, T. (2020). Anatomical and electrophysiological analysis of cholinergic inputs from the parabigeminal nucleus to the superficial superior colliculus. *Journal of Neurophysiology*, *124*(6), 1968-1985.

Van Horn, S. C., Erişir, A., & Sherman, S. M. (2000). Relative distribution of synapses in the A-laminae of the lateral geniculate nucleus of the cat. *Journal of Comparative Neurology*, *416*(4), 509-520.

Varoqui, H., Schäfer, M. K. H., Zhu, H., Weihe, E., & Erickson, J. D. (2002). Identification of the differentiation-associated Na+/PI transporter as a novel vesicular glutamate transporter expressed in a distinct set of glutamatergic synapses. *Journal of Neuroscience*, *22*(1), 142-155.

Wang, Y. Q., Takatsuji, K., Kiyama, H., Yamano, M., & Tohyama, M. (1988). Localization of neuroactive substances in the rat parabigeminal nucleus: an immunohistochemical study. *Journal of chemical neuroanatomy*, *1*(4), 195-204.

Watanabe, M., & Rodieck, R. W. (1989). Parasol and midget ganglion cells of the primate retina. *Journal of Comparative Neurology*, *289*(3), 434-454.

Wiberg, M., & Blomqvist, A. (1984). The projection to the mesencephalon from the dorsal column nuclei. An anatomical study in the cat. *Brain research*, *311*(2), 225-244.

Wiberg, M., Westman, J., & Blomqvist, A. (1987). Somatosensory projection to the mesencephalon: an anatomical study in the monkey. *Journal of Comparative Neurology*, *264*(1), 92-117.

Zénon, A., & Krauzlis, R. J. (2012). Attention deficits without cortical neuronal deficits. *Nature*, *489*(7416), 434-437.

Zhang, H. Y., & Hoffmann, K. P. (1993). Retinal projections to the pretectum, accessory optic system and superior colliculus in pigmented and albino ferrets. *European Journal of Neuroscience*, *5*(5), 486-500.

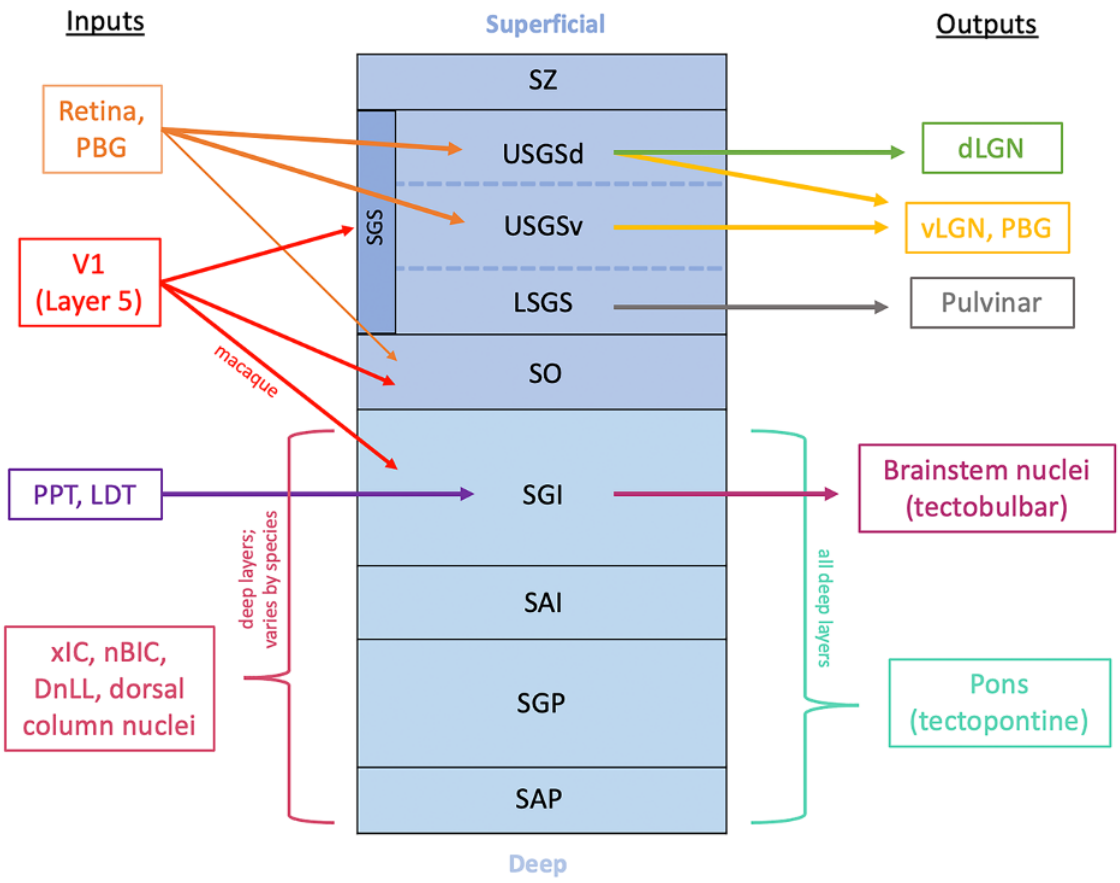

Figure 1. Laminar organization of mammalian superior colliculus (SC) is shown with each layer's corresponding inputs (left) and outputs (right), where the thickness of each arrow corresponds to the density of innervation. The seven main layers of the SC are labeled: zonal layer (SZ); superficial gray layer (SGS), which in tree shrews is further subdivided into the dorsal upper SGS (USGSd), ventral upper SGS (USGSv), and lower SGS (LSGS); optic layer (SO); intermediate gray layer (SGI); intermediate white layer (SAI); deep gray layer (SGP); and deep white layer (SAP). These layers are functionally segregated into two divisions: a dorsally located visuosensory division (dark blue), consisting of the SZ, upper and lower SGS, and SO, and a ventrally located motor division (light blue), consisting of the SGI, SAI, SGP, and SAP (Sparks & Hartwich-Young, 1989; May, 2006). The superficial layers of the SC are specialized to receive retinal information, with retinotectal projections terminating primarily in the SGS and minimal terminations in SO (Graybiel, 1975 [cat]; Pollack & Hickey, 1979 [monkey]; Lund et al., 1980 [rat]). The visuosensory layers follow a segregated pattern, where more dorsally located neurons in the upper SGS project to the LGN, while more ventrally located neurons, in the lower SGS and SO, project to pulvinar (Benevento & Standage, 1983). Selective corticotectal projections provide input to SGS and SO (Huerta et al., 1985 [tree shrew]; Harting, Updyke, & Van Lieshout, 1992 [cat]; Lui et al., 1995 [primate]), and only extend to layers beneath SO in macaques, where projections extend to SGI (Lui et al., 1995). The cholinergic parabigeminal nucleus (PBG) inputs provide dense innervation of the retinorecipient layers (Graybiel, 1978; Tokuoka et al., 2020), while the pedunculopontine tegmentum (PPT) and laterodorsal tegmental nucleus (LDT) provide cholinergic input to the SGI (Fitzpatrick et al., 1988; Hall et al., 1989). The motor layers of the SC receive multisensory information, including auditory and somatosensory signals. Auditory inputs to SC vary by species, however, the external nucleus of the inferior colliculus (xIC), nucleus of the brachium of the inferior colliculus (nBIC), and the nuclei of the dorsal lateral lemniscus (DnLL) comprise the majority of projections in most species, including primates (Edwards et al., 1979; Druga & Syka, 1984; Jiang et al., 1997). Somatosensory connections come from the brainstem and spinal cord, with dorsal column nuclei projecting onto the deep layers of the SC (Wiberg & Blomqvist, 1984; Wiberg, Westman, & Blomqvist, 1987).

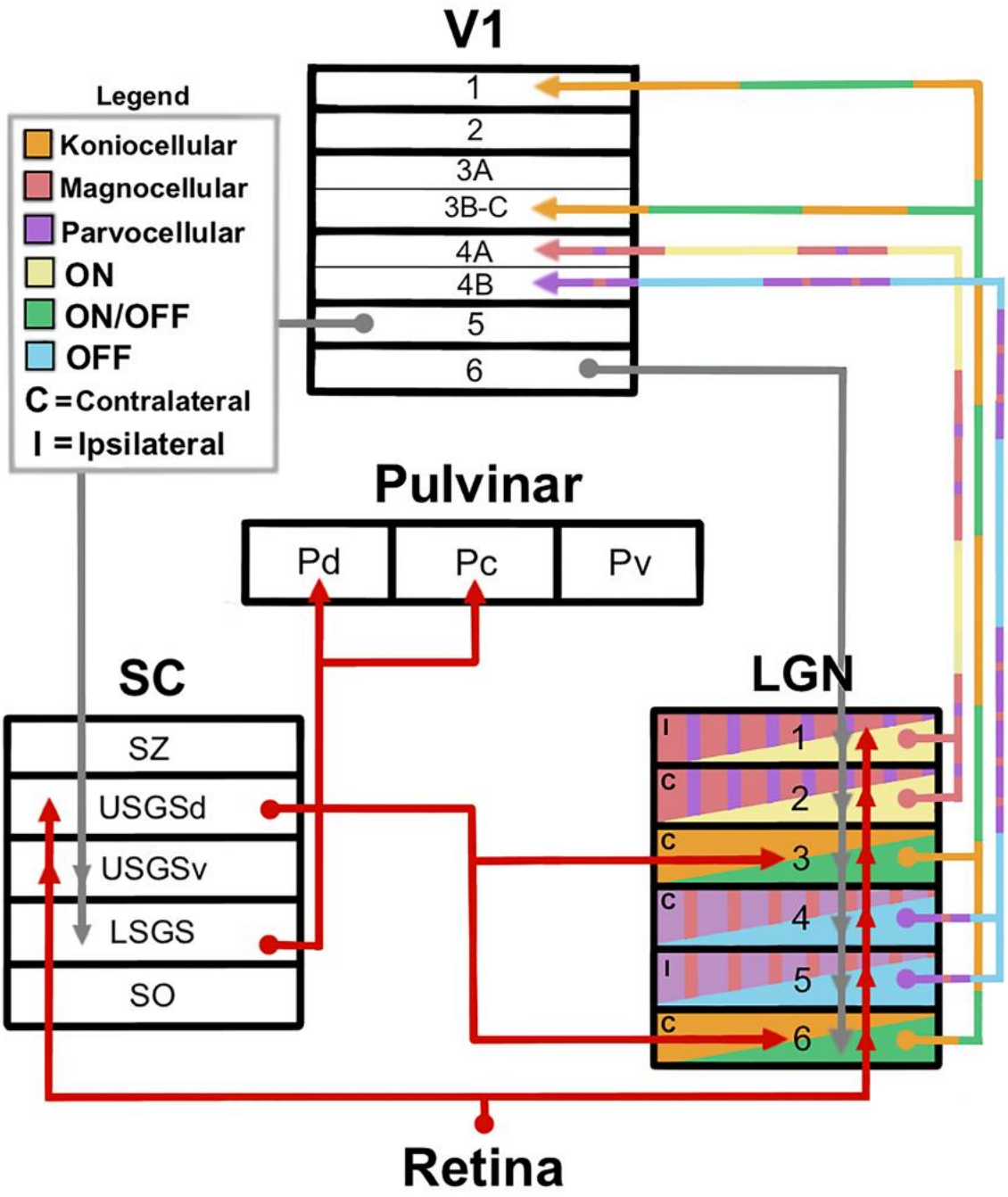

Figure 2. Parallel pathway segregation in the tree shrew dLGN is shown. Organization of the tree shew dLGN parallel pathways contain three pairs of layers: laminae 1 and 2, laminae 4 and 5, and laminae 3 and 6. The dorsal upper SGS (USGSd) is specialized to receive retinal input and projects to laminae 3 and 6 of dLGN, which both receive contralateral (C), koniocellular (orange), and ON/OFF (green) input. Legend is shown in the upper left with the colors and letters that correspond to their respective parallel processing streams.

Table 1. Antibodies used in this study.

Antibody name	Immunogen	Antibody info	Dilution
Anti-vesicular glutamate transporter 2 (VGLUT2)	KLH-conjugated linear peptide corresponding to the C-terminal sequence of rat VGLUT2.	EMD Millipore Corporation; Cat# AB2251; RRID:AB_1587626; Guinea Pig (Polyclonal)	1:2500
Biotin anti-Guinea Pig IgG	-	Vector; Cat# BA-7000; Goat (polyclonal)	1:50

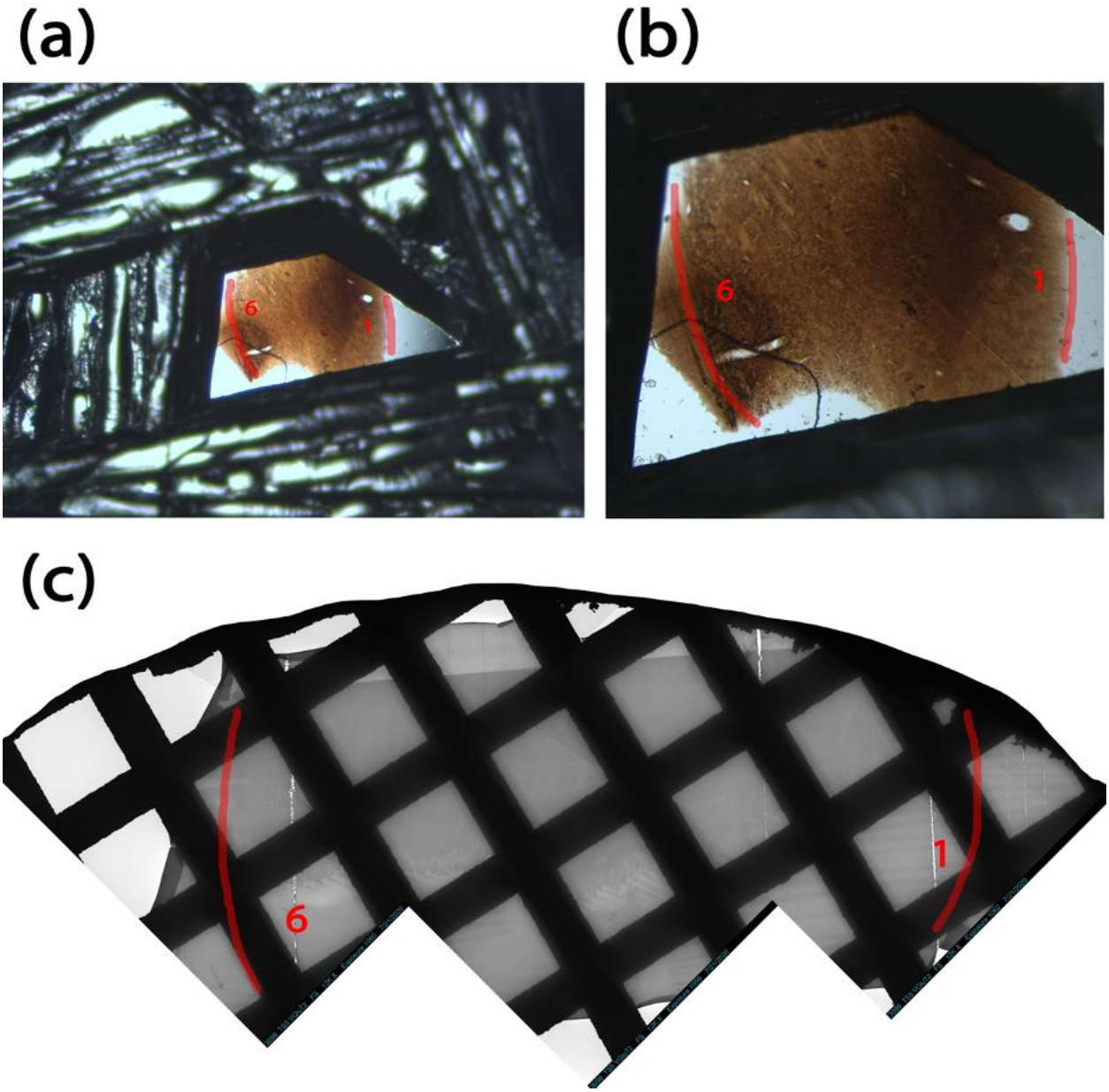

Figure 3. (a) A capsule with the entirety of the dLGN is trimmed down to a trapezoid before ultrathin sectioning at 1.6X magnification. The region of interest is traced and major landmarks are included to help orient the tissue in later steps of EM processing. (b) Trapezoid at 5X magnification. After finding the optic tract, we know that lamina 6 is immediately adjacent to these myelinated axons and its location is marked for reference. Once the location of lamina 6 is determined, we're able to use other landmarks and the approximate size of dLGN to determine the location of lamina 1, which is also marked. (c) Trapezoid on copper grid imaged with an electron microscope at 120X magnification. We are able to use landmarks and regions determined in panels a and b to orient the tissue at higher magnifications.

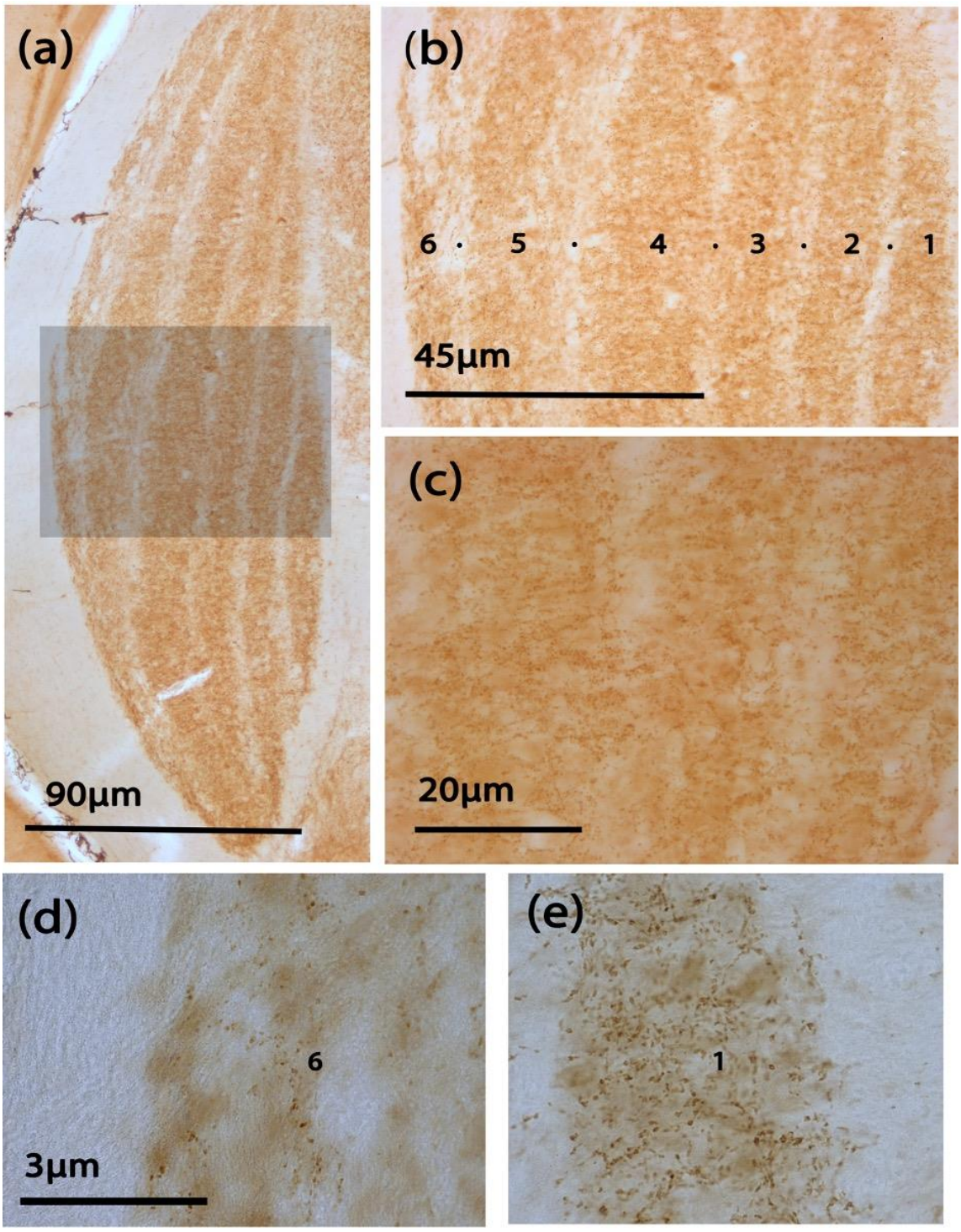

Figure 4. Immunolabeling with VGLUT2 antibody reveals clearly defined laminae of the tree shrew dLGN. (a) All geniculate laminae shown at 5X magnification; box corresponds to area shown at higher magnifications in the remaining panels. (b) Geniculate laminae at 10X magnification, where lamina 1 is most medial and lamina 6 is most lateral; dots indicate interlaminar zones. (c) Laminae 2 (right), 3 (center), and 4 (left) at 20X magnification. (d) Lamina 6 at 40X magnification reveals more sparse VGLUT2 labeling. (e) Lamina 1 at 40X magnification reveals more diffuse VGLUT2 labeling; scale is the same as in panel d.

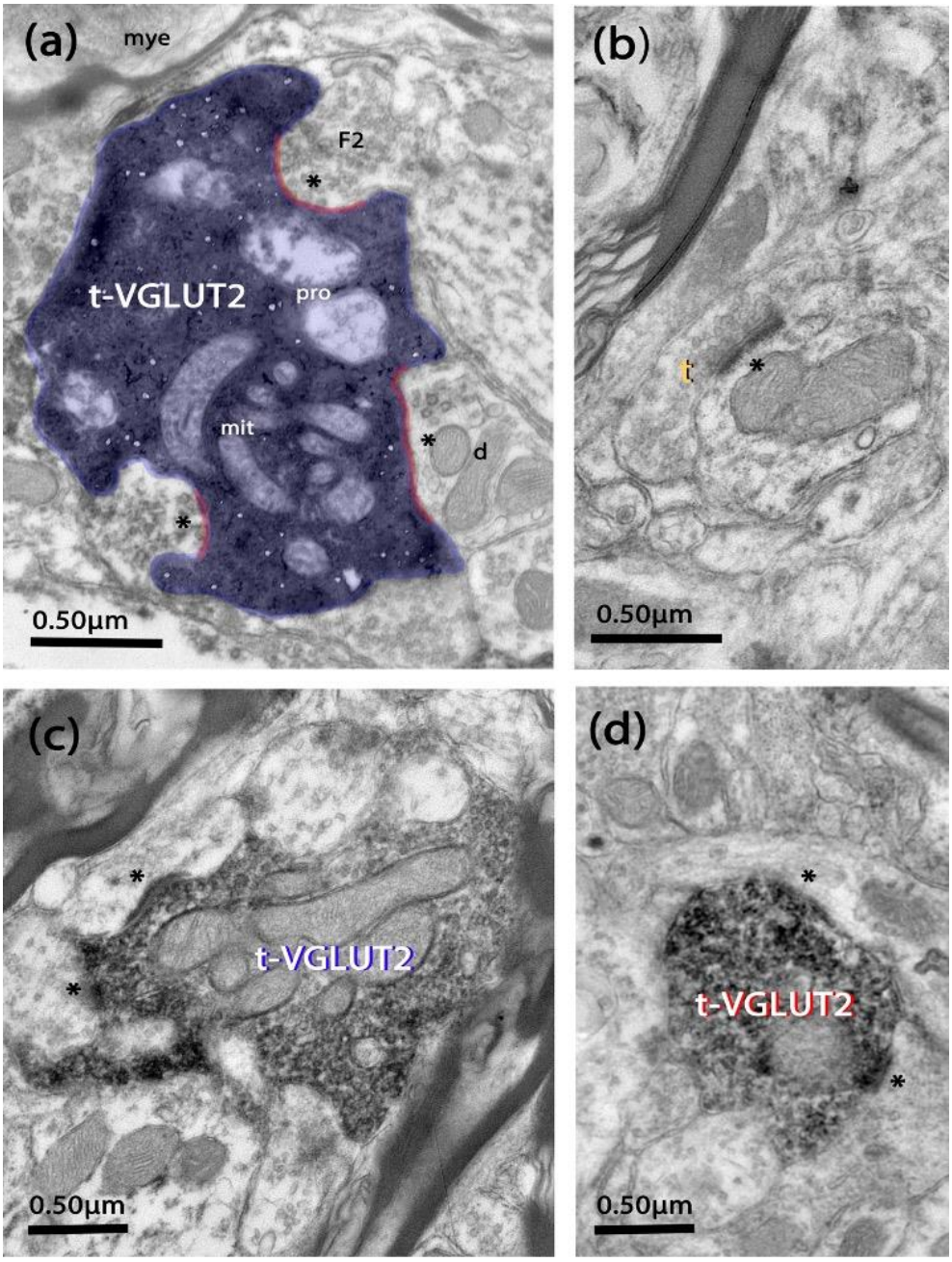

Figure 5. Electron micrographs in the tree shrew dorsal lateral geniculate nucleus (dLGN). (a) For analyses, labeled and unlabeled terminals were outlined to calculate their area (blue) and each synapse was traced to calculate length (red) and the asterisk (*) marks the synapse at the postsynaptic side, here and in all subsequent panels; this terminal (t-VGLUT2) makes multiple synapses onto a dendrite (d) and a vesicle-filled profile (F2; classified as such because it contains pleomorphic vesicles and is postsynaptic to another terminal). (b) An unlabeled terminal in lamina 1 (t, yellow), synapsing onto a dendrite, contains round vesicles and no mitochondria. (c) A large terminal in lamina 1 (t-VGLUT2, blue), labeled with VGLUT2 antibody, contains several mitochondria and visible protrusions and makes multiple synapses. (d) A smaller terminal in lamina 6 (t-VGLUT2, red), labeled with VGLUT2 antibody, contains few mitochondria and makes multiple synapses. Electron micrographs were obtained at 12kX magnification for all panels.

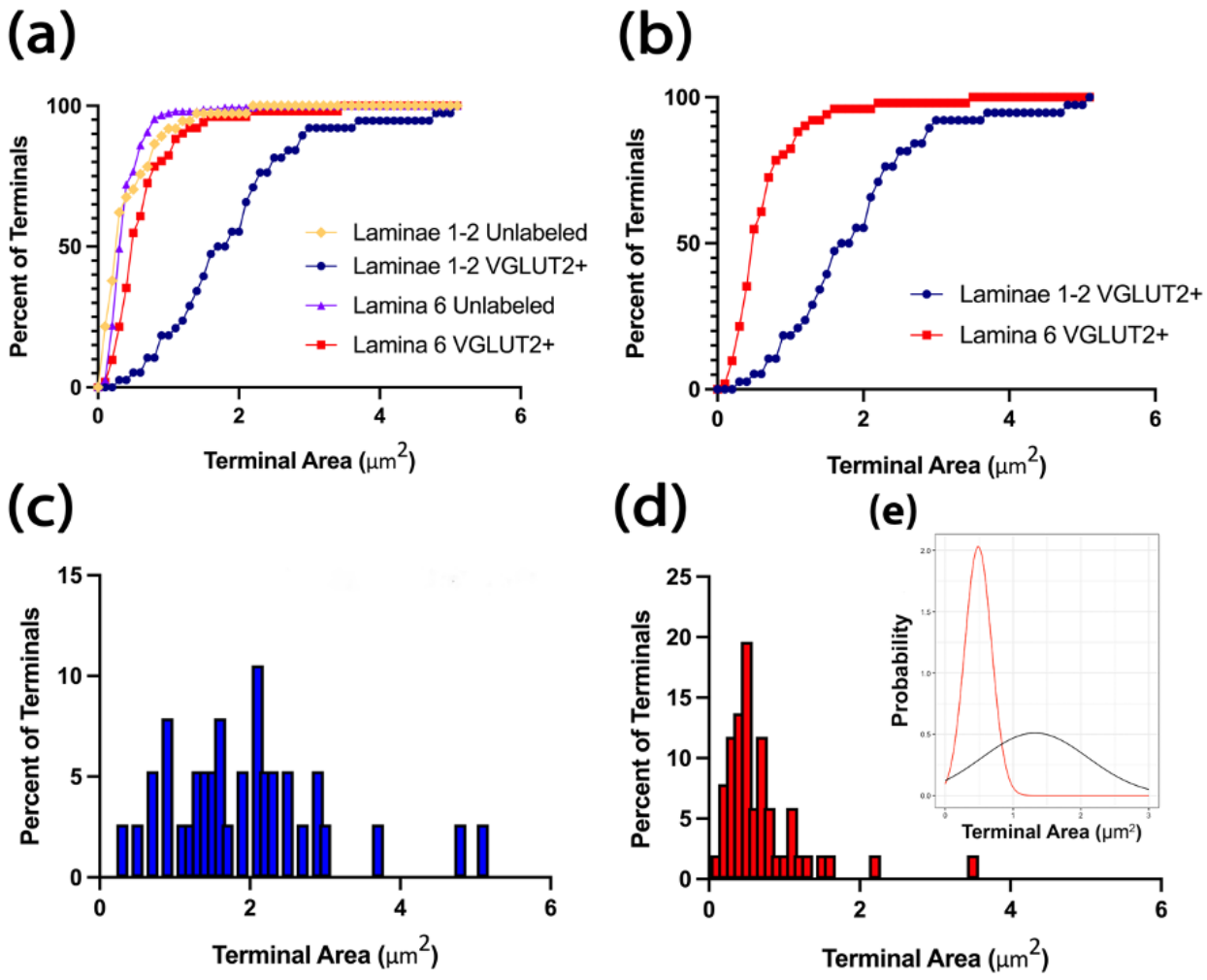

Figure 6. Terminal area distributions of koniocellular vs. magno/parvo laminae**.** (a) The distribution histograms of terminal bouton area of all VGLUT2 population terminals, including unlabeled terminals from laminae 1-2 (yellow), VGLUT2+ terminals from laminae 1-2 (blue), unlabeled terminals from lamina 6 (purple), and VGLUT2+ terminals from lamina 6 (red), in the tree shrew dLGN. (b) The distribution histograms of terminal bouton area of VGLUT2+ terminals in laminae 1-2 (blue) and lamina 6 (red) in the tree shrew dLGN. (c) The size distribution histogram VGLUT2+ terminals in laminae 1 and 2. (d) The size distribution histogram of VGLUT2+ terminals in lamina 6. (e) Two subpopulations of VGLUT2+ terminals in lamina 6, revealed by a BIC analysis (R-MClust), are fitted as curves and plotted in different colors.

Table 2. Targeting properties of VGLUT2+ terminals in koniocellular vs. magnocellular/parvocellular laminae and TG terminals in laminae 3 and 6.

	VGLUT2+ Terminals in Laminae 1 and 2 (n = 66)	VGLUT2+ Terminals in Lamina 6 (n = 57)	TG Terminals in Laminae 3 and 6 (n = 18)
Dendritic shafts	56.06%	38.60%	61.11%
Vesicle-filled profiles	10.61%	42.10%	22.22%
Protrusions	33.33%	19.30%	16.67%

Table 3. Synaptic properties of VGLUT2+ terminals in koniocellular vs. magnocellular/parvocellular laminae and TG terminals in laminae 3 and 6.

	VGLUT2+ Terminals in Laminae 1 and 2 (n = 38)	VGLUT2+ Terminals in Lamina 6 (n = 45)	TG Terminals in Laminae 3 and 6 (n = 18)
Protrusions	52.63%	20.00%	-
Triad	18.42%	46.67%	22.22%
Makes 1 Synapse	57.89%	80.00%	100%
Makes 2-3 Synapses	34.21%	20.00%	-
Makes >3 Synapses	7.89%	-	-

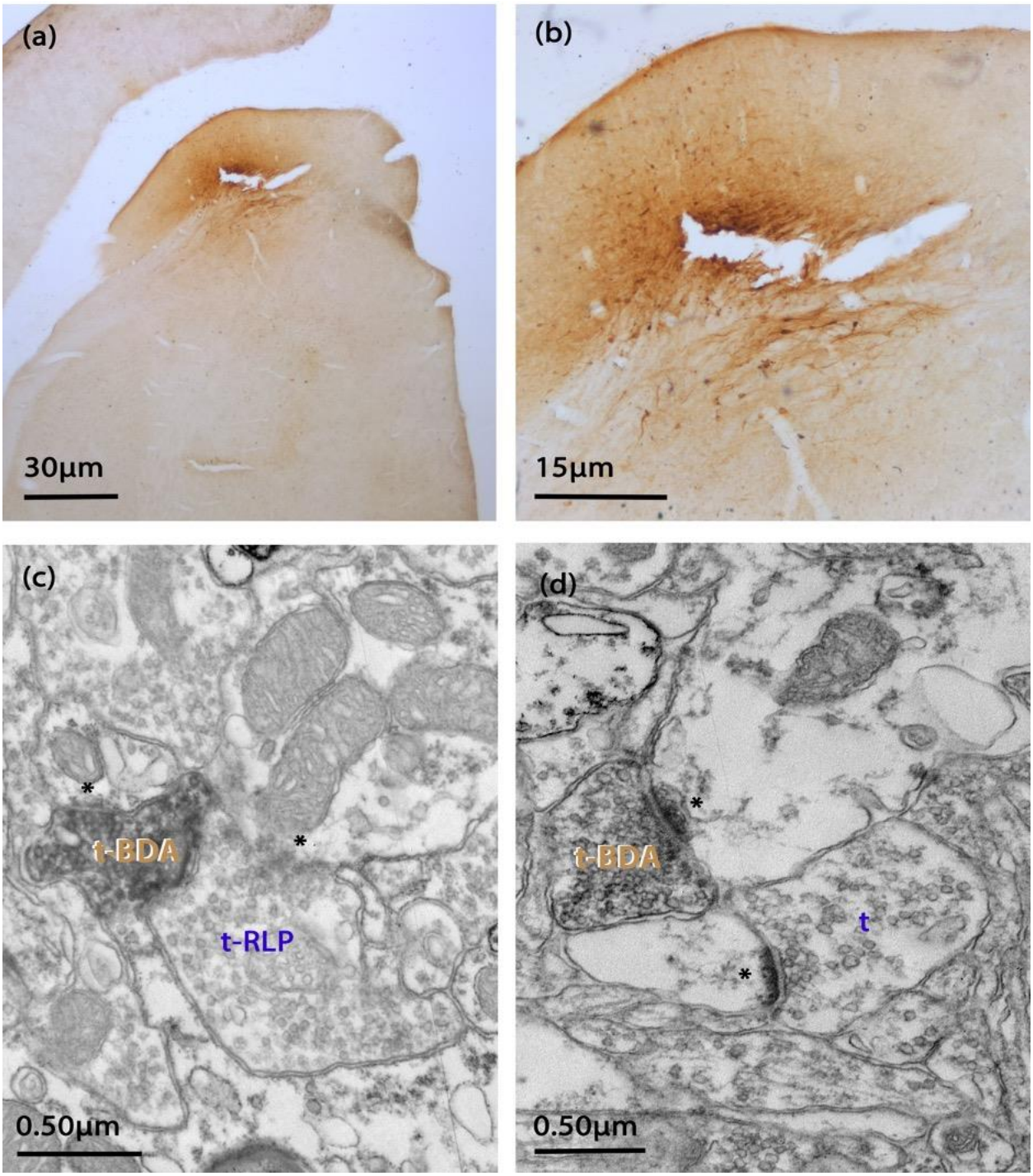

Figure 7. (a) Injection site of the BDA anterograde tracer into the superficial SC shown at 1.6X magnification. (b) Injection site shown at 5X magnification, where labeled fibers are shown. (c) A small terminal in lamina 3 (t-BDA), anterogradely filled with BDA, next to RLP (t-RLP; determined by large size, round vesicles, and visibly pale mitochondria) obtained at 12kX magnification. (d) A small terminal in lamina 6 (t-BDA), anterogradely filled with BDA, next to an unlabeled terminal (t) obtained at 15kX magnification.

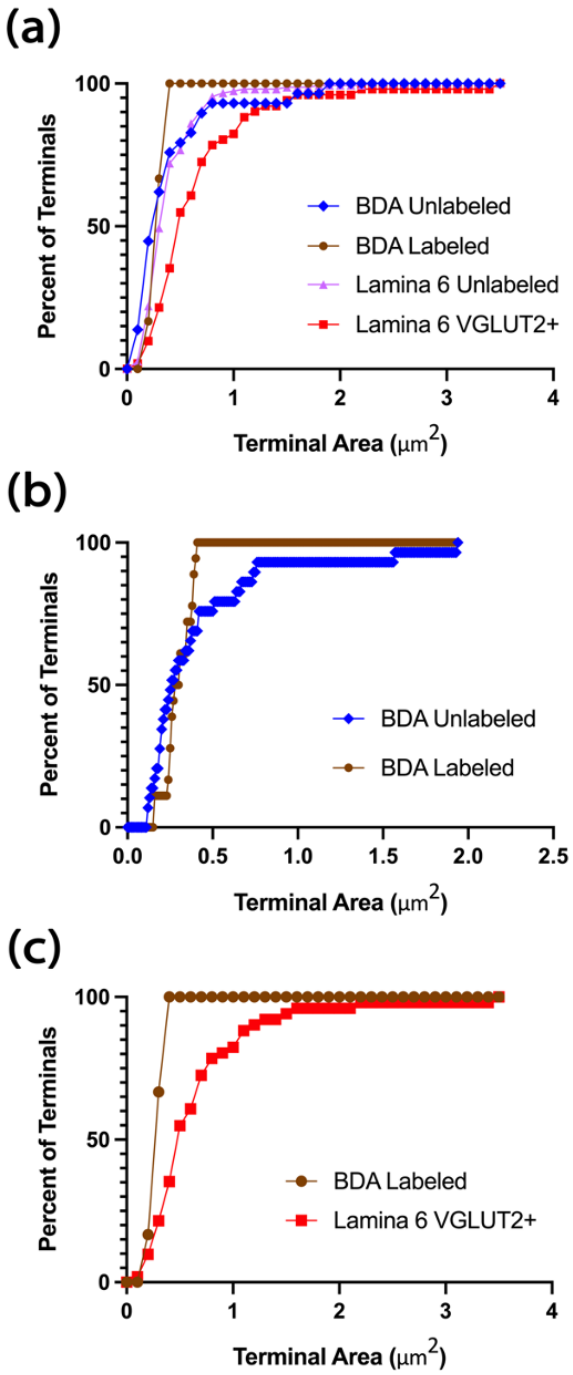

Figure 8. (a) The distribution histograms of terminal bouton area of both VGLUT2 and BDA population terminals, including BDA-unlabeled terminals in laminae 3 and 6 (blue), BDA-labeled terminals in laminae 3 and 6 (brown), VGLUT2-unlabeled terminals in lamina 6 (purple), and VGLUT2+ terminals in lamina 6 (red), in the tree shrew dLGN. (b) The distribution histograms of terminal bouton area of BDA-unlabeled (blue) and labeled (brown) terminals in laminae 3 and 6 of the tree shrew dLGN. (c) The distribution histograms of terminal bouton area of BDA-labeled terminals in laminae 3 and 6 (brown), and VGLUT2+ terminals in lamina 6 (red), in the tree shrew dLGN.

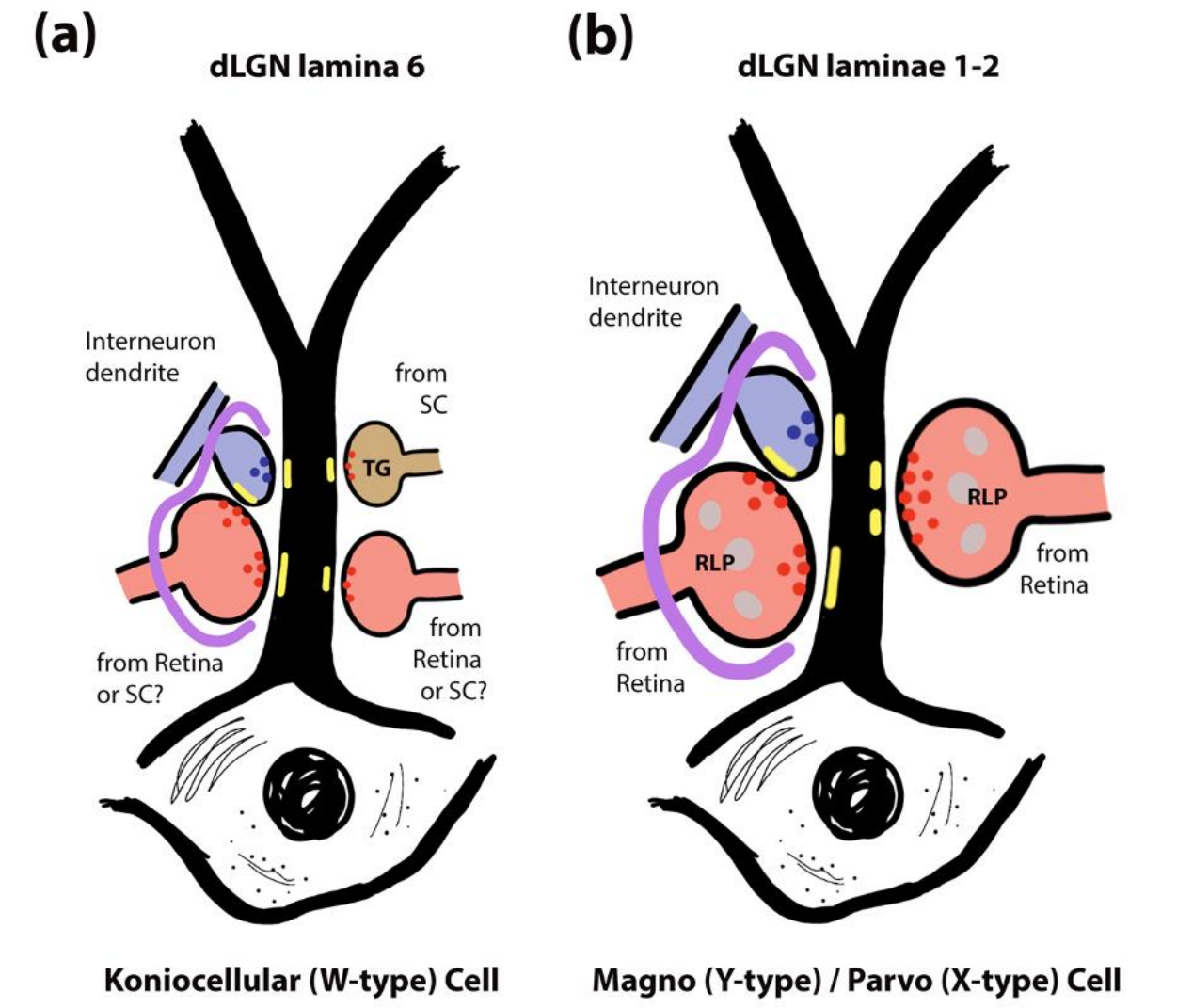

Figure 9. Schematic comparison of synaptic inputs onto relay cell dendrites in the dLGN of (a) koniocellular (W-type) cells in lamina 6, and (b) magnocellular (Y-type)/parvocellular (X-type) cells in laminae 1-2. A characteristic of retinal terminals are glia (purple) encased glomerular triads involving the primary sensory input and presynaptic interneuron dendrites (blue), which were seen in both sets of laminae but more frequently in koniocellular lamina 6. Protrusions (gray circles), another characteristic of retinal terminals, were seen more frequently in VGLUT2+ terminals (red) in magno/parvo laminae and less frequently in koniocellular lamina 6. VGLUT2+ terminals in koniocellular lamina 6 showed a multimodal distribution of small and large terminals that were primarily monosynaptic. Contrastingly, VGLUT2+ terminals in magno/parvo laminae showed larger terminals that preferentially targeted dendritic shafts and made multiple synaptic contacts (yellow). TG terminals (brown) are only present in koniocellular laminae and are significantly smaller than RLPs, show no protrusions, and are monosynaptic.